Dai *et al.*
Chinese Journal of Mechanical Engineering (2022) 35:8
https://doi.org/10.1186/s10033-021-00670-4

Chinese Journal of Mechanical Engineering

ORIGINAL ARTICLE

Open Access

Precise Compound Control of Loading Force for Electric Load Simulator of Electric Power Steering Test Bench

Changhua Dai[2], Guoying Chen[2*], Changfu Zong[2] and Buyang Zhang[1]

Abstract

Electric load simulator (ELS) systems are employed for electric power steering (EPS) test benches to load rack force by precise control. Precise ELS control is strongly influenced by nonlinear factors. When the steering motor rapidly rotates, extra force is directly superimposed on the original static loading error, which becomes one of the main sources of the final error. It is key to achieve ELS precise loading control for the entire EPS test bench. Therefore, a three-part compound control algorithm is proposed to improve the loading accuracy. First, a fuzzy proportional–integral plus feedforward controller with force feedback is presented. Second, a friction compensation algorithm is established to reduce the influence of friction. Then, the relationships between each quantity and the extra force are analyzed when the steering motor rapidly rotates, and a net torque feedforward compensation algorithm is proposed to eliminate the extra force. The compound control algorithm was verified through simulations and experiments. The results show that the tracking performance of the compound control algorithm satisfies the demands of engineering practice, and the extra force in the ELS system can be suppressed by the net torque corresponding to the actuator's acceleration.

Keywords: Electric load simulator, Electric power steering, Extra force, Compound control

1 Introduction

With excellent dynamic loading performance, the use of an electric load simulator (ELS) is an important loading method for electric power steering (EPS) test benches. Currently, well-known supplement suppliers, such as IABG and IPG, provide accurate rack force for EPS test benches by controlling ELS loading [1]. ELS is a typical nonlinear system, and the loading process is influenced by friction, damping, and backlash [2]. In addition, because it is a passive loading system, extra force is inevitably generated in ELS when the steering motor rapidly rotates [3]. Extra force is directly superimposed on the original static loading error and becomes one of the main sources of the final error. The test performance of the EPS system depends largely on the ELS loading accuracy. Therefore, it is crucial to improve ELS loading accuracy for the entire EPS test bench.

To improve the loading accuracy of ELS, offline manual adjustment and online automatic control are the two generally adopted methods. In engineering practices, ELS can achieve high loading accuracy after repeated offline manual adjustments for specific working conditions. However, this method is time-consuming and laborious, and it is not suitable for variable working conditions. In the field of academic research, online automatic control has become the main choice. Previous studies [4, 5] proposed a proportional controller and analyzed the stability of the control process. In other studies, a smooth switching fuzzy proportional–integral–derivative (PID) controller was proposed, and the algorithm was verified experimentally [6], and an adaptive robust torque

*Correspondence: cgy-011@163.com
[2] State Key Laboratory of Automotive Simulation and Control, Jilin University, Changchun 130022, China
Full list of author information is available at the end of the article

controller was applied [7–11]. At the same time, a fuzzy neural network controller was applied [12, 13]. Both control algorithms have excellent performance. In another study [2], a variable structure wavelet neural network recognition strategy based on adaptive differential evolution was used. A few researchers [14, 15] proposed a cerebellar joint model proportional–derivative (PD) hybrid controller that avoids overlearning. For friction nonlinear factors, various friction models have been proposed, such as a continuous friction model based on smooth shape function [11], Lugre friction model [6, 16], friction model focusing on low speed [15], and the friction model designed in other studies [17, 18]. Elimination of extra force is divided into two modes: by hardware and software. In the hardware mode, damping elements are installed between the steering motor and the sensor [19]. However, the mode requires sophisticated structural design. In the software mode, different compensation algorithms have been proposed. In previous research [6, 9, 11], feedforward compensation algorithms were proposed based on the velocity. A few studies [7, 8] adopted a fuzzy-logic compensation method, and a high-order error dynamic reverse step controller was proposed [16] to compensate for the extra force influence.

In this work, a novel precise compound control algorithm is proposed to improve ELS loading accuracy for the EPS test bench. The algorithm consists of three parts. First, to improve the loading accuracy, a fuzzy proportional–integral (PI) plus feedforward controller based on force feedback is proposed. Next, to reduce the influence of system friction, the design of a friction compensation algorithm based on the Lugre friction model is described. The force error and the load motor's velocity are considered in the friction compensation algorithm. Then, the influences on ELS loading accuracy are analyzed when the steering motor rapidly rotates, and the state quantities are placed under the same coordinate axis. The trends of extra force, the steering motor's acceleration, and the net torque corresponding to the rack acceleration are similar. At the same time, when the steering motor rapidly rotates, the precise real-time acceleration is difficult to obtain by the velocity differential or an acceleration sensor, while the net torque corresponding to the rack acceleration is easily calculated by each feedback force. Therefore, a net torque feedforward compensation algorithm is proposed to suppress the extra force. The compound control algorithm was verified through simulations and experiments. The results show that the tracking performance of the compound control algorithm satisfies the demands of engineering practice.

This work is organized as follows. In Section 2, the model of the EPS test bench is described. In Section 3, the compound control algorithm is detailed. The simulations in MATLAB/Simulink are discussed in Section 4, where test results are presented and analyzed. Section 5 includes the conclusions.

2 Mathematical Modeling

Figure 1 shows the system structure of the EPS test bench divided into six parts: a force sensor, a combination of a load motor and speed reduction mechanism, a combination of a column and rack, a torque sensor, an assist motor, and a steering motor. The combination of the load motor and the speed reduction mechanism is the ELS system. The steering motor and the load motor are driven by motor drivers. The PXI controller completes the computational instruction of each motor driver and provides information to the PC.

The steering motor proactively provides the power of movement for the EPS system. The steering motor is a permanent magnet synchronous motor controlled by a position servo through a motor driver. Without considering the controller and the friction of the steering motor, the steering motor's electric and torque balance equation is described as

$$u_s = L_s\dot{I}_s + R_sI_s + C_s\omega_s, \tag{1}$$

$$T_s = J_s\dot{\omega}_s + B_s\omega_s + T_t, \tag{2}$$

$$T_s = K_sI_s, \tag{3}$$

where L_s is the inductance of the steering motor, R_s is resistance, C_s is the back-electromotive-force (EMF) coefficient of the steering motor, J_s is the rotational inertia of the steering motor, B_s is the damping coefficient of the steering motor armature, T_t represents the torque of the torque sensor, and K_s is the torque coefficient of the steering motor.

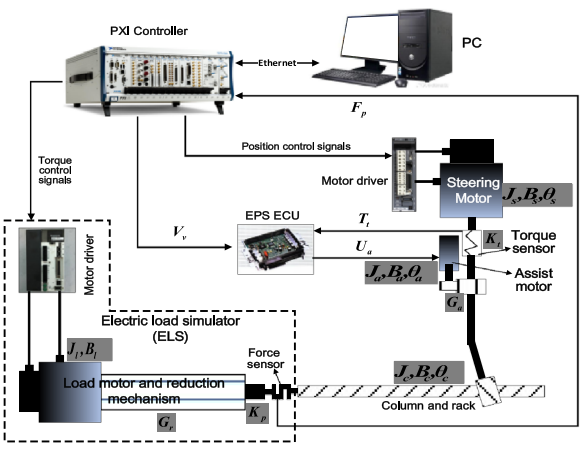

Figure 1 System structure of EPS test bench

The torque sensor's deformation is linear with the torque, so the equation ignoring the damping coefficient of sensor is

$$T_t = K_t(\theta_s - \theta_c), \tag{4}$$

where K_t is the stiffness coefficient of the torque sensor, and θ_s and θ_c are the angles of rotation of the steering motor and column.

The assist motor is regarded as an armature-controlled DC motor [20]. The effective voltage signal, u_a, that drives the assist motor electrical circuit can be expressed as

$$u_a = L_a\dot{I}_a + (R_a + R_f)I_a - K_a\omega_a, \tag{5}$$

where, L_a indicates the inductance of the assist motor, R_a and R_f are the resistances of the armature circuit and the current feedback, and K_a is the back-EMF constant of the assist motor.

Connected with the column by a gear pair, the assist motor's torque is enlarged through the transmission ratio. The assist torque shown on the column is

$$T_m = G_aK_iI_a, \tag{6}$$

where, G_a indicates the ratio of the assist gear pair, and K_i is the assist motor torque constant.

The column is rotated by the power from the steering and assist motors, and it is regarded as a part of the combination with the rack. As a combination, after the rotational inertia and damping coefficient of rack are converted to the column, the torque balance equation should be

$$T_t + T_m = J_c\dot{\omega}_c + B_c\omega_c + T_l, \tag{7}$$

$$T_l = F_Pr_P\eta_P, \tag{8}$$

where J_c is the rotational inertia of the combination of column and rack, B_c is the damping coefficient of the combination of column and rack, T_l represents the torque of the pinion, F_P is the force of the force sensor, r_P is the radius of the pinion, and η_P represents the effectiveness of the pinion pair.

The force sensor's deformation is linear with the force. The real-time force is gathered from the force sensor, which is depicted as

$$F_P = K_P(\theta_cG_P - \theta_lG_r), \tag{9}$$

where K_P is the stiffness of the force sensor, θ_c is the rotation angle of the column, G_P represents the ratio of the pinion, θ_l is the rotation angle of the load motor, and G_r denotes the ratio of the reduction mechanism.

Finally, the combination of the load motor and the reduction mechanism is the same as for the steering motor except for the mechanical parameters and friction of the combination, for which the influence of the reduction mechanism should be considered. Therefore, after the rotational inertia and damping coefficient of the reduction mechanism are converted to the load motor, its electric and torque balance equation is described as

$$u_l = L_l\dot{I}_l + R_lI_l + C_l\omega_l, \tag{10}$$

$$T_l = J_l\dot{\omega}_l + B_l\omega_l + (F_P + F_f)r_r\eta_r, \tag{11}$$

$$T_l = K_lI_l, \tag{12}$$

where, L_l is the inductance of the load motor, R_l is the resistance and C_l is the back-EMF coefficient of the load motor, J_l is rotational inertia and B_l is the damping coefficient of the combination of the load motor and reduction mechanism, F_f represents the friction of the combination of the load motor and reduction mechanism, r_r is the equivalent radius of the reduction mechanism, η_P represents the inverse effectiveness of the combination of the load motor and reduction mechanism, and K_l is the torque coefficient of the load motor.

The current loop proportion of the steering motor is defined as K_{vs}, and load motor's current loop proportion is defined as K_{vl}. The current control gains are defined as K_{Ps} and K_{Pl}, and the current feedback coefficients are defined as K_{fs} and K_{fl}. Considering the load force controller with force feedback, the block diagram of the entire test bench can be depicted as Figure 2.

3 Precise Compound Control of Loading Force

As shown in Figure 3, the novel compound control algorithm consists of three terms: a fuzzy-PI plus feedforward controller, a friction compensation algorithm, and a net torque feedforward compensation algorithm. The final force multiplies a force voltage coefficient K_{Fv}, to transform to a target voltage. The target voltage is shown as V_l in Figure 2.

3.1 Fuzzy-PI Plus Feedforward Controller

It is difficult to satisfy the precision demand when PID controllers are used, because PID controllers are linear and have been incapable of providing good control over highly nonlinear systems [21]. A fuzzy controller is suitable for nonlinear systems [22, 23] because of its outstanding robustness and fault tolerance, and it can offset the uncertainty of those parameters of the test bench.

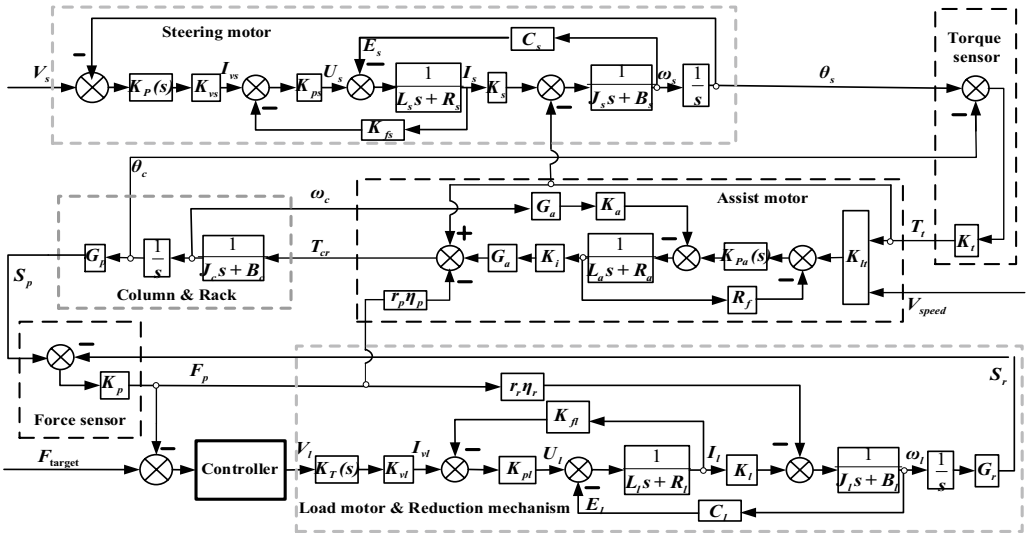

Figure 2 Block diagram of ELS of an EPS test bench

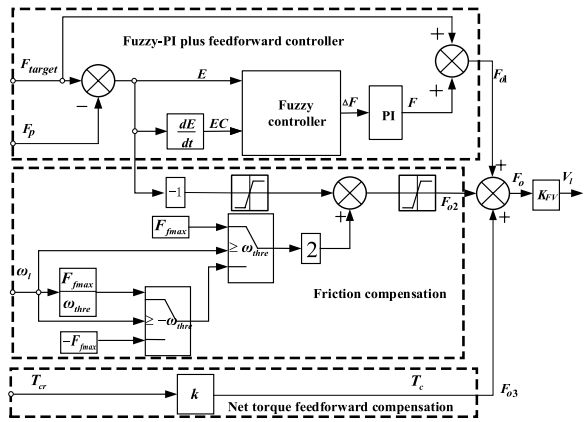

Figure 3 Block diagram of compound control algorithm

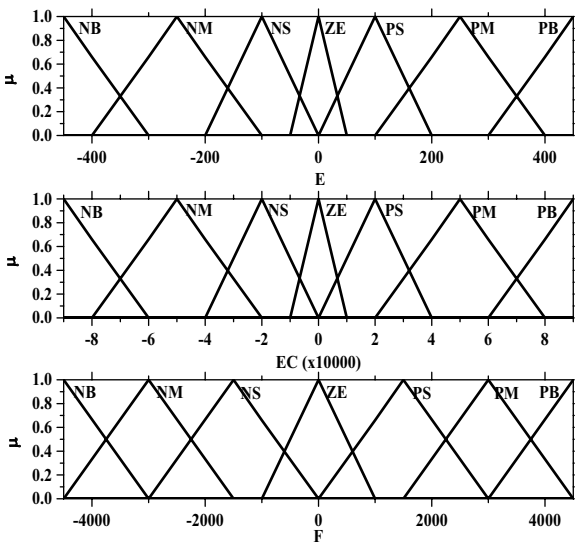

Figure 4 Corresponding membership function of force error, rate of force error change, and output of fuzzy controller

Because of the lack of integral terms, it is easy for a fuzzy controller to generate steady-state static error [24, 25]. For this situation, a novel combined controller that considers the two factors is presented as the structure shown in Figure 3.

A double-input fuzzy controller is employed, and its inputs include the force error and the rate of force error change. The output of the fuzzy controller is an increment. The steps for the fuzzy controller are as follows.

First, the force error and the rate of force error change need to be processed to meet the fuzzy control requirements.

Next, the corresponding membership function has been depicted in Figure 4. The rules of the fuzzy controller are shown in Table 1. Finally, the value of output is as shown in Figure 4.

Next, an integral term is employed to compensate the steady-state error of the fuzzy controller. A method in which the output increment of the fuzzy controller is used as the input of the PI controller is presented. To play the role of fuzzy controller, the proportion parameter of the PI controller is set to 1. Here, the PI controller just plays the role of introducing an integral term for the fuzzy controller.

Then, as a feedforward term, the target force superimposes on the fuzzy-PI controller's output considering the dynamic response of controller. Theoretically, the

Table 1 Rules of fuzzy controller

EC	E						
	NB	NM	NS	ZE	PS	PM	PB
NB	NB	NB	NM	NM	NS	ZE	ZE
NM	NB	NB	NM	NS	NS	ZE	PS
NS	NM	NM	NM	NS	NM	PS	PS
ZE	NM	NM	NS	ZE	PS	PM	PM
PS	NS	NS	ZE	PS	PS	PM	PM
PM	NS	ZE	PS	PM	PM	PM	PB
PB	ZE	ZE	PM	PM	PM	PB	PB

combined controller is rapid and adaptive in terms of the feedforward and fuzzy controller. Its integration term keeps the accuracy of control. Therefore, the output F_{o1}, of the combined controller can be described as

$$F_{o1}(t) = F_{target}(t) + p \cdot \Delta F(t) + i \cdot \frac{1}{T} \cdot \int_0^t \Delta F(t)\, \mathrm{d}t, \tag{13}$$

where F_{target} is the value of the target load force, ΔF represents the output increments of the fuzzy controller, and p and i are the proportion and integral term parameters of the PI controller.

3.2 Friction Compensation Control

Friction is the largest factor to influence the ELS precise loading control. Lugre friction is the most common model used in engineering practice [26, 27]. To reduce the adverse effects of system friction, a friction compensation algorithm is proposed based on the model of Lugre friction shown in Figure 5.

The friction model facilitates the process from static friction to dynamic friction. First, the force error is the static friction when the load motor is static. Second, considering the movement of the load motor, double linear friction compensation is added on the force error. It is used to eliminate the influence of the load motor movement on the process that, from static friction, transforms to dynamic friction. Finally, a threshold of the friction output is set up to reach the Lugre friction model's requirement. The expression can be presented as follows.

When $|F_f| < F_{f\max}$ (area 1 shown in Figure 5), its expression is

$$F_{f1} = \begin{cases} F_e + 2\left|\frac{F_{f\max}}{\omega_{thre}}\right| \cdot \omega_l, \ |F_e| < F_{f\max} \& |\omega_l| < |\omega_{thre}|, \\ F_e + 2F_{f\max} \cdot \mathrm{sign}(\omega_l), \ |F_e| < F_{f\max} \& |\omega_l| \geq |\omega_{thre}|, \\ F_{f\max} \cdot \mathrm{sign}(F_e) + 2\left|\frac{F_{f\max}}{\omega_{thre}}\right| \cdot \omega_l, \ |F_e| \geq F_{f\max} \& |\omega_l| < |\omega_{thre}|, \\ F_{f\max} \cdot \mathrm{sign}(F_e) + 2F_{f\max} \cdot \mathrm{sign}(\omega_l), \ |F_e| \geq F_{f\max} \& |\omega_l| \geq |\omega_{thre}|. \end{cases} \tag{14}$$

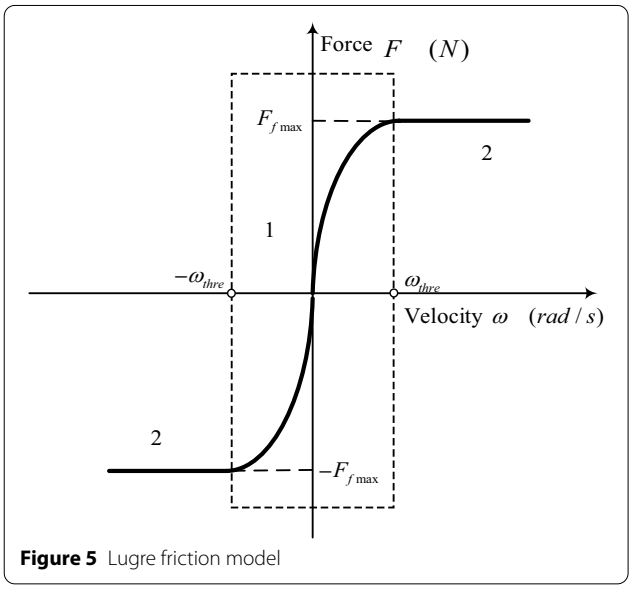

Figure 5 Lugre friction model

$$F_{o2} = F_{f1}. \tag{15}$$

When $|F_f| \geq F_{f\max}$ (area 2 shown in Figure 5), its expression is

$$F_{o2} = F_{f\max} \cdot \mathrm{sign}(F_{f1}), \tag{16}$$

where F_{o2} is the output value of friction compensation, F_e is defined as the force error, ω_{thre} represents the threshold of velocity, $F_{f\max}$ means the maximum of static friction, and the function, sign(), takes a positive or negative sign of the quantity.

3.3 Net Torque Feedforward Compensation Control

In the EPS test bench, the steering motor rotates through the position servo, which makes the rack linear move with the help of the assist motor. At the same time, the load motor provides rack force following the rack movement through the force sensor. However, the rapid rack movement is a disturbance to the precision of load force control. Extra force is generated in this procedure. Extra force is the peak and valley of force error generated after the fuzzy-PI plus feedforward controller and the friction compensation algorithm are used when the steering motor rapidly rotates.

In Figure 6 under a step steering condition, the simulation results without control, including the steering angle, rack velocity, rack acceleration, sensor force, extra force, and net torque, are shown. Considered the target force and the actual sensor force, the existence of extra force can be illustrated. The correlations between the extra force and steering angle or the rack velocity cannot be perfunctorily and simply recognized. However, the rack acceleration's trend nearly coincides with the extra force's trend. Movement is generated later than velocity, and velocity is generated later than acceleration. Therefore, under such rapid movement disturbance, the force sensor has been forced before the rack moves. This suggests that extra force is affected greatly by the rack acceleration when the load motor precisely executes the signals from the computer.

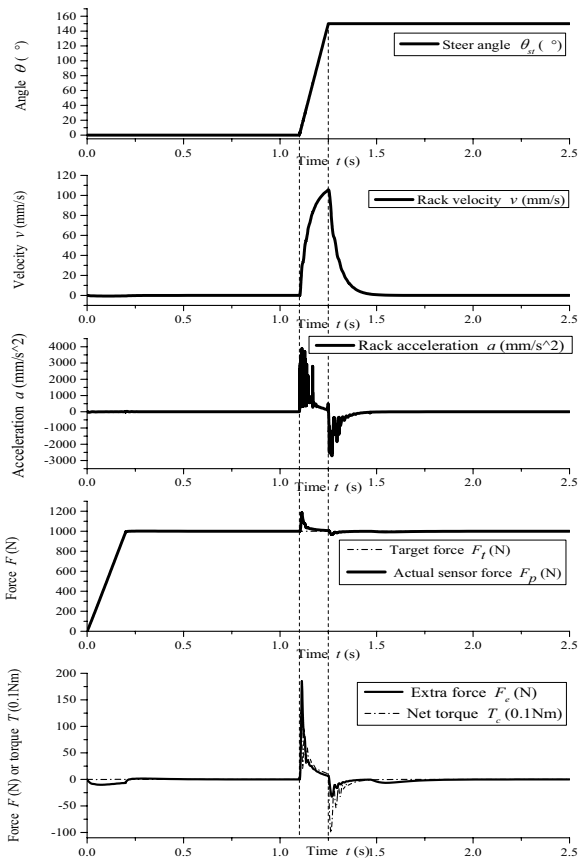

Figure 6 Simulation results without control under step steering condition

The above-mentioned inference suggests that the rack acceleration is multiplied by a gain to feedforward compensate. The compensation, F_c, is shown as

$$F_c = K_c a, \tag{17}$$

where K_c is the compensation gain, and a represents the rack acceleration.

When the steering motor rapidly rotates, the precise real-time acceleration is difficult to obtain by the velocity differential or an acceleration sensor. However, the trend of net torque corresponding the rack acceleration nearly coincides with the trend of extra force as well. The net torque is defined as T_{cr}, depicted in Figure 2.

$$T_{cr} = J_c \dot{\omega}_c, \tag{18}$$

$$a = \dot{\omega}_c r_P. \tag{19}$$

Analyzing Eqs. (18) and (19), the net torque can be regarded as the acceleration multiplied by a constant gain. The net torque is easy to obtain by calculating the value of the torque sensor, the EPS assist force, and the force sensor. The net torque is real time and always generates earlier than the rack movement. Therefore, the net torque substituting for the acceleration becomes the basis of compensation. This suggests that the net torque is multiplied by a gain k to feedforward compensate. The compensation, F_{o3}, can be depicted as

$$F_{o3} = kT_{cr}. \tag{20}$$

Extra force is eliminated by the net torque compensation with apposite parameters. Extra force is supposed as F_{e1}, and the relationship of extra force and the net torque compensation can be depicted as

$$G_s F_{o3} + F_{e1} = 0, \tag{21}$$

where, G_s is the transfer function of the combination of the load motor and the speed reduction mechanism.

4 Simulation and Experimental Results

4.1 Simulation Results

A simulation model based on the mathematical model was built in MATLAB/Simulink, where the map of EPS

assist torque was adopted from a B-classed car on the CARSIM. A steering condition was designed, where the target force was set to 1 kN, and the steering motor steered 150° within 0.15 s, since the 1.1th second under a vehicle speed of 60 km/h. In addition, the sliding friction of the ELS model was set to ±500 N. Three simulation results are shown, and they respectively verify the fuzzy-PI plus feedforward controller, the friction compensation algorithm, and the net torque feedforward compensation algorithm. Table 2 lists the key parameters of the entire model.

To verify individually the tracking performance of the fuzzy-PI plus feedforward controller and provide a comparable object, the friction compensation and the net torque feedforward compensation were not employed in the simulation. The result is shown in the Figure 7. The remaining part, except the period of steering, nearly coincides with the target force. Peak A is generated when the steering motor starts to rotate, and valley B is generated when steering motor brakes. The value of peak A is far greater than the value of valley B, because peak A needs more power to generate accelerations starting from a static state.

At the same time, simulation employing only a pure PID controller was done for comparison with the fuzzy-PI plus feedforward controller. The PID controller's proportion, integral, and differential term parameters were, respectively, set as 10, 10, and 0.001. The result is shown in Figure 8.

The comparison of Figures 7 and 8 shows that the value of peak A reduces by more than 46% and the value of valley B reduces by more than 79% when the fuzzy-PI plus feedforward controller is employed. In addition,

Table 2 Key parameters of simulation model

Signal	Value/Unit	Signal	Value/Unit
$K_{vs}(K_{vl})$	1.74 A/V	J_s	0.000304 kg·m^2
$K_{Ps}(K_{Pl})$	10 V/A	K_t	1000 N·m·rad
$K_s(K_l)$	0.8218 N·m/A	R_f	0.1 Ω
$K_{fs}(K_{fl})$	1	L_a	0.00012 H
$L_s(L_l)$	0.0012 H	B_s	0.00202 N·m·s/rad
$R_s(R_l)$	1.53 Ω	R_a	0.2 Ω
$C_s(C_l)$	0.2779 V·s/rad	K_a	1 V/N·m
G_a	16.5 mm/rad	K_i	0.0151 N·m/A
J_c	0.0255 kg·m^2	B_c	0.038 N·m·s/Rad
G_P	6.3694	K_P	10029 N/mm
r_P	0.005 m	η_P	100%
J_l	0.00290 kg·m^2	B_l	0.0102 N·m·s/rad
r_r	0.001 mm	η_P	80%
G_r	5 mm/rad	ω_{thre}	0.5 rad/s
$F_{f\,max}$	500 N	k_{FV}	0.001 V/N
p	1	i	8

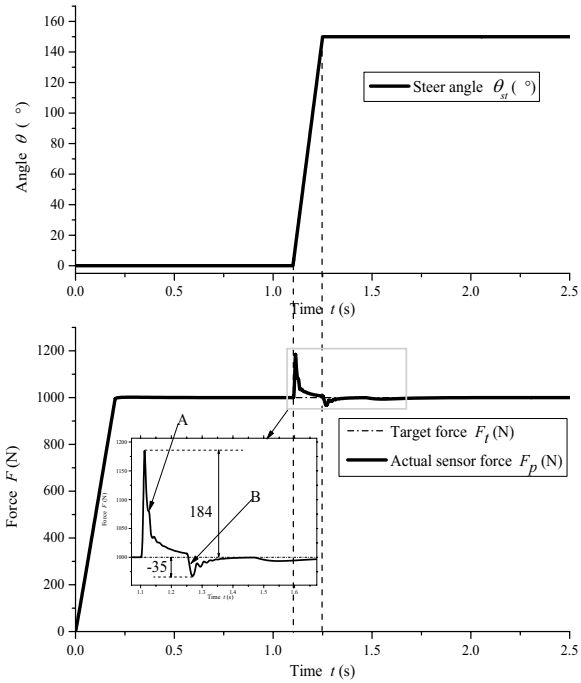

Figure 7 Tracking performance of the fuzzy-PI plus feedforward controller under step steering condition

the tracking performance is worse with a larger tracking error, and the force flutters with high frequency in the magnified area when the PID controller is used, which indicates that the control process under the PID controller is less stable than that under the fuzzy-PI plus feedforward controller.

As shown in Figure 9, the effectiveness of the friction compensation was verified by employing friction compensation and the fuzzy-PI plus feedforward controller, and without the net torque feedforward compensation.

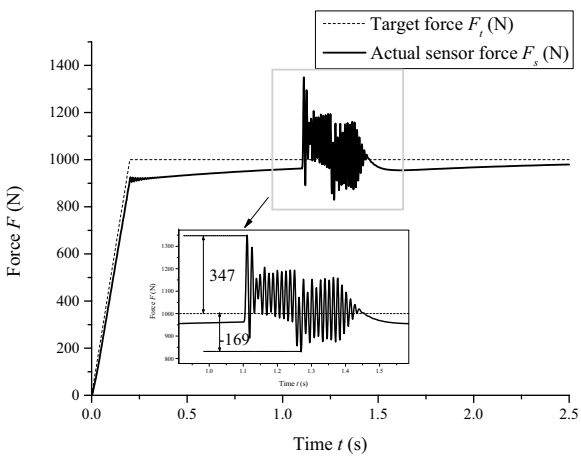

Figure 8 Tracking performance of the PID controller under step steering condition

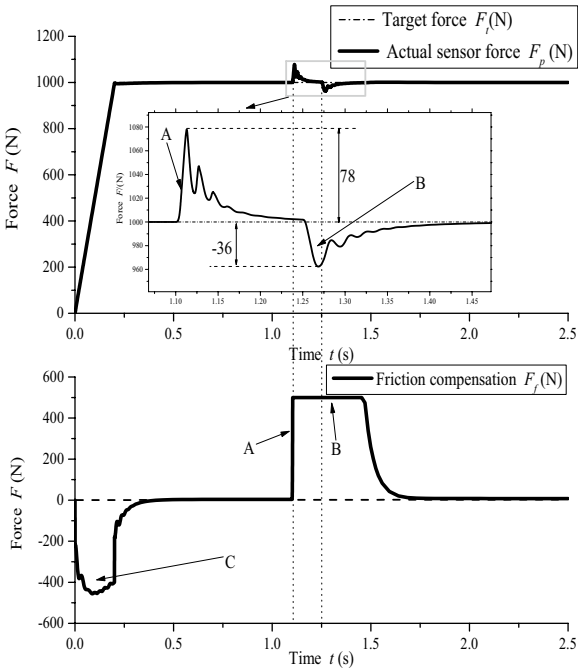

Figure 9 Tracking performance of friction compensation and fuzzy-PI plus feedforward controller under step steering condition

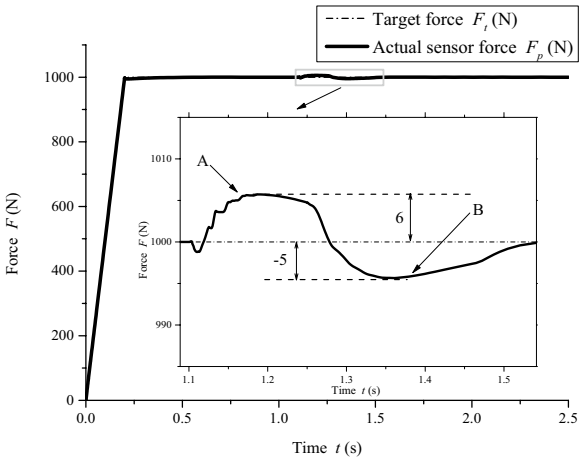

Figure 10 Tracking performance of compound control algorithm under step steering condition

Comparison of Figures 7 and 9 shows that the friction compensation reduces the value of peak A by more than 56%, while there is little change of the value of valley B. When the steering motor starts to rotate, the friction compensation makes a step change to compensate for part A. That leads to the reduction of peak A. When the steering motor brakes, the friction compensation does not change, which is shown as part B. At this moment, the friction compensation just compensates for the steady-state error in part B. Because the test bench is not absolutely rigid, there are a slight rack movement and force error when the load force starts to increase from zero. Thus, the friction compensation is generated during part C.

As shown in Figure 10, the effectiveness of the compound control algorithm was verified by employing the net torque feedforward compensation and all the other algorithms. Comparison of Figures 9 and 10 shows that the value of peak A reduced to 6 from 78 and the value of valley B reduced to −5 from −36 when the net torque compensation algorithm was employed. As analyzed in Section 2, the trends of extra force and the net torque were similar, and peak A and valley B simultaneously existed in extra force and the net torque. Therefore, the extra force was reduced by the net torque compensation with apposite parameters. Comparison of Figures 7 and 10 shows that the value of peak A decreased by more than 97% and the value of valley B decreased by more than 85% when the compound algorithm was employed.

4.2 Experimental Results

An EPS test bench was built, and it is shown in Figure 11, where the test bench includes the steering motor, the EPS system, the rack steering, and the load motor.

In this test bench, the EPS system is the tested part rather than the developed part, and it provides the assist torque, as in normal cars. At the same time, the load motor provides the rack force replacing the steering tires.

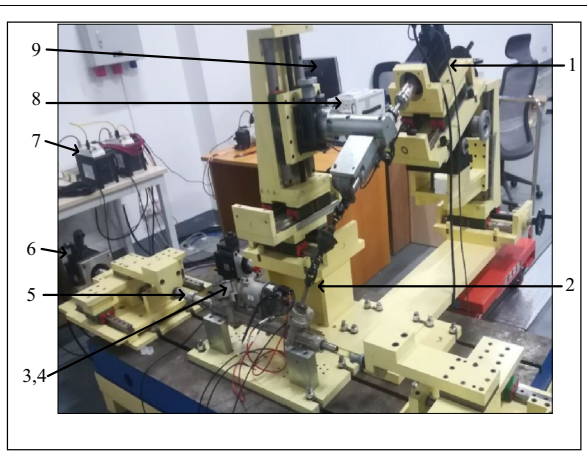

Figure 11 EPS test bench: 1. Steering motor; 2. Column and rack; 3. Torque sensor; 4. Assist motor; 5. Force sensor; 6. Load motor and speed reduction mechanism; 7. Motor driver; 8. PXI controller; 9. Computer

4.2.1 Verification of Fuzzy-PI Plus Feedforward Controller with Force Feedback

Experiment 1 was designed to verify individually the tracking performance of the fuzzy-PI plus feedforward controller when employed in a static condition. In experiment 1, the steering motor was braked as a static object. The target rack force gained from CARSIM is shown in Figure 12. The result of the test experiment is shown in Figure 12 as well.

Figure 12 shows that the actual sensor force nearly coincides with the target force, and its maximum error is 7%, satisfying the demands of engineering practice.

4.2.2 Verification of Extra Force Suppression Control by Net Torque Feedforward Compensation Algorithm

Experiment 2 was designed to verify the effectiveness of the net torque feedforward compensation. In experiment 2, the steering motor drove the entire bench as a steering wheel. The steering motor rotated with a sine condition, whose amplitude was set to 180° and frequency was set to 1 Hz. The target rack force was set to zero, while the net torque was obtained by calculating the values of the torque sensor, the EPS assist motor, and the force sensor. The net torque feedforward compensation algorithm and other algorithms were used from beginning to the 10th second, while the result without the net torque feedforward compensation algorithm was generated from the 10th to the 17th second. The actual sensor force of experiment 2 can be regarded as extra force and is shown in Figure 13.

In Figure 13, a comparable performance is shown, where the extra force was reduced to 322 N from 749 N with the net torque feedforward compensation. With the load motor as a physical part, the loading accuracy was nearly 200 N. The load motor's physical loading accuracy was hardly improved by the control algorithms. Because the results were based on the motor physical loading accuracy, the improved performance of the net torque feedforward compensation algorithm was far more than 56%.

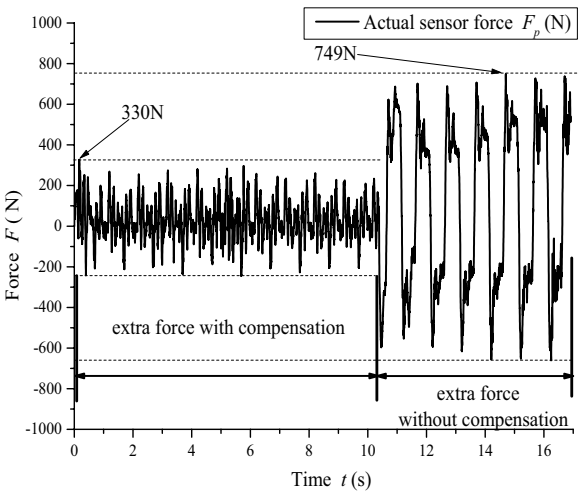

Figure 13 Actual sensor force of experiment 2

4.2.3 Verification of the Compound Control Algorithm

Experiment 3 was designed to verify the tracking performance of the compound control algorithm comprehensively when it was employed in a dynamic condition. In experiment 3, the steering motor rotated according to the target steering angle, which is shown in Figure 14. The target rack force gained by the CARSIM is shown in Figure 15. The result of experiment 3 is shown in Figure 15 as well.

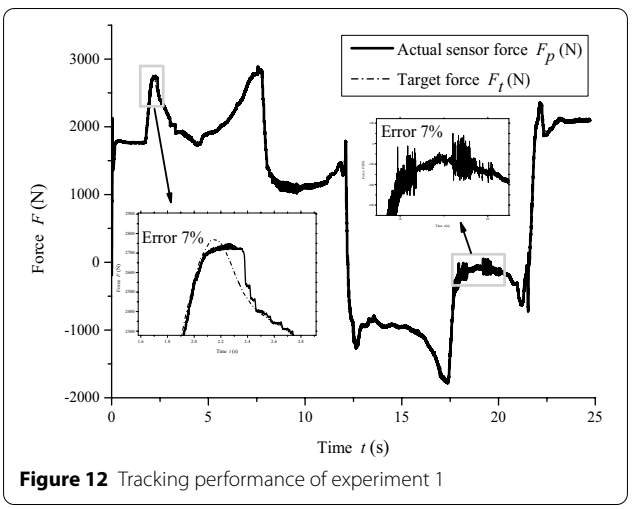

Figure 12 Tracking performance of experiment 1

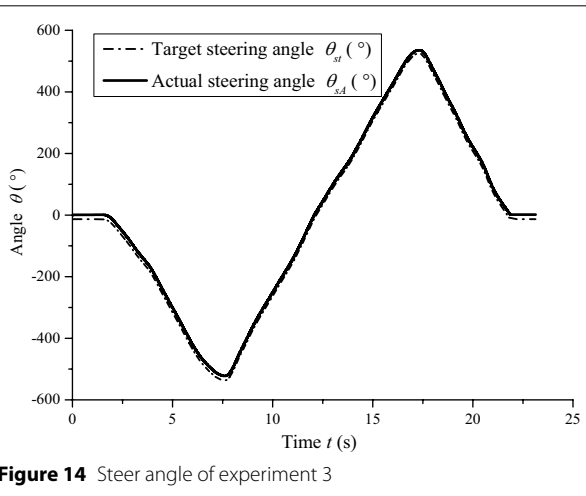

Figure 14 Steer angle of experiment 3

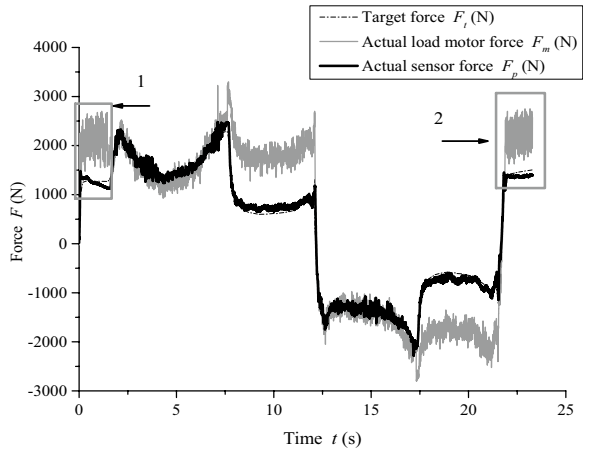

Figure 15 Tracking performance of experiment 3

Figure 15 shows that the actual load motor force deviated from the target force and the actual sensor force in some periods. Owing to the existence of friction, the actual load motor force deviated from the actual sensor force when the rack was static, which is shown as areas 1 and 2, and this proved the validity of the friction control algorithm. There were many disturbances on the actual load motor force. The combination of the load motor and speed reduction mechanism can be regarded as a low-pass filter because of the friction and damping. The high-frequency noise was partly suppressed when the actual load motor force passed through the low-pass filter. Therefore, the actual sensor force under small noise nearly coincided with the target force.

5 Conclusions

A compound control algorithm was proposed with the fuzzy-PI plus feedforward controller superimposed on the friction compensation algorithm and the net torque compensation algorithm. The control algorithms were verified by simulations and experiments.

(1) The efficacy of the fuzzy-PI plus feedforward controller is sufficient for the tracking performance of the control in such a nonlinear system.
(2) The friction compensation algorithm considering the force error and the load motor movement is suitable for the ELS system.
(3) The sensor force is the result of the collective effect of the load motor and the steering motor, and the extra force can be reduced if the net torque drives the column and rack. This suggests that the extra torque can be reduced by the net torque corresponding to the acceleration of the actuator in the ELS system.
(4) Comprehensive experimental investigation shows that the tracking performance of the compound control algorithm satisfies the demands of engineering practice, and this provides a foundation for the testing of EPS systems.

Acknowledgements
Not applicable.

Authors' Contributions
CD was in charge of the whole trial; CD wrote the manuscript; CD and GC assisted with sampling and laboratory analyses. CZ reviewed the manuscript. BZ guided journal submissions. All authors read and approved the final manuscript.

Authors' Information
Changhua Dai, born in 1995, is currently a PhD candidate at *College of Automotive Engineering, Jilin University, China*. His research interests include automotive dynamics simulation and control.
Guoying Chen, born in 1984, is an associate professor at *State Key Laboratory of Automotive Simulation and Control, Jilin University, China*. His research interests include automotive dynamics simulation and control.
Changfu Zong, born in 1962, is a professor at *State Key Laboratory of Automotive Simulation and Control, Jilin University, China*. His research interests include automotive dynamics simulation and control.
Buyang Zhang, born in 1989, is currently a PhD at *College of Automotive Engineering, Jilin University, China*. His research interests include vehicle dynamic, vehicle stability control, intelligent tire, non-pneumatic tire.

Funding
Supported by National Natural Science Foundation of China (Grant No. 51505178) and China Postdoctoral Science Foundation (Grant No. 2014M561289).

Competing Interests
The authors declare no competing financial interests.

Author Details
[1]College of Automotive Engineering, Jilin University, Changchun 130022, China. [2]State Key Laboratory of Automotive Simulation and Control, Jilin University, Changchun 130022, China.

Received: 8 June 2020 Revised: 23 April 2021 Accepted: 21 December 2021
Published online: 12 February 2022

References

[1] H O Xiang. *Development and verification of hardware-in-loop test bench for electrically controlled steering system*. Changchun: Jilin University, 2014.
[2] C Wang, Y L Hou, R Z Liu, et al. The identification of electric load simulator for gun control systems based on variable-structure WNN with adaptive differential evolution. *Applied Soft Computing*, 2016, 38: 164-175.
[3] G Y Chen, L He, C F Zong, et al. A Research on the resistance loading strategy for steering test bench based on motor serco system. *Automotive Engineering*, 2018, 40(2): 226-233.
[4] L S Wang, M Y Wang, B Guo. Analysis and design of a speed controller for electric load simulators. *IEEE Transactions on Industrial Electronics*, 2016, 63(12): 7413-7422.
[5] L S Wang, M Y Wang, B Guo, et al. A loading control strategy for electric load simulators based on proportional resonant control. *IEEE Transactions on Industrial Electronics*, 2018, 56(6): 4608-4618.

[6] X J Wang, S P Wang, X D Wang. Electrical load simulator based on velocity-loop compensation and improved fuzzy-PID. *IEEE International Symposium on Industrial Electronics*, Seoul, South Korea, 5-8 July, 2009: 238-243.
[7] N Ullah, S P Wang, J Aslam. Adaptive robust control of electrical load simulator based on fuzzy logic compensation. *Proceedings of 2011 International Conference on Fluid Power and Mechatronics,* Beijing, China, 17-20 Aug., 2011.
[8] N Ullah, S P Wang. Torque controller design for electrical load simulator with estimation and compensation of parametric uncertainty. *Proceedings of 2012 9th International Bhurban Conference on Applied Sciences & Technology (IBCAST)*, Islamabad, Pakistan, 9-12 Jan., 2012: 15-21.
[9] X J Wang, S P Wang, B Yao. Adaptive robust torque control of electric load simulator with strong coupling disturbance. *International Journal of Control, Automation and Systems*, April 2013, 11(2): 325-332.
[10] X J Wang, S P Wang. High performance torque controller design for electric load simulator. *Industrial Electronics & Applications*, 2011: 2499-2505.
[11] X J Wang, S P Wang, P Zhao. Adaptive fuzzy torque control of passive torque servo systems based on small gain theorem and input-to-state stability. *Chinese Journal of Aeronautics*, 2012, 25(6): 906-916.
[12] L Wang, L F Qian, Q Guo. Torque control of servo load simulator with generalized dynamic fuzzy neural network based on grey prediction. *Applied Mechanics and Materials*, December 2011, 148-149: 707-712.
[13] B Guo, M Y Wang, J Zhang. A dynamic fuzzy neural networks controller for dynamic load simulator. *International Conference on Machine Learning and Cybernetics*, Dalian, China, 13-16 Aug., 2006.
[14] B Yang, H T Han, R Bao. An intelligent CMAC-PD torque with anti-over-learning scheme for electric load simulator. *Transactions of the Institute of Measurement & Control*, Feb. 2016, 38(2): 192-200.
[15] B Yang, R Bao, H T Han. Robust hybrid control based on PD and novel CMAC with improved architecture and learning scheme for electric load simulator. *IEEE Transactions on Industrial Electronics*, 2014, 61(10): 5271-5279.
[16] N Ullah, S P Wang. Higher order error dynamics based backstepping controller design for electrical load simulator. *Proceedings of 2013 10th International Bhurban Conference on Applied Sciences & Technology (IBCAST)*, Islamabad, Pakistan, 15-19 Jan. 2013.
[17] S L Han, K S Lee. Robust friction state observer and recurrent fuzzy neural network design for dynamic friction compensation with backstepping control. *Mechatronics*, 2010, 20(3): 384-401.
[18] I B Tijani, R Akmeliawati. Support vector regression-based friction modeling and compensation in motion control system. *Engineering Application of Artificial Intelligence*, August 2012, 25(5): 1043-1052.
[19] R Li. Research on control system of motor-driven load simulator. Taiyuan: North University of China, 2013.
[20] R Ghimire, C Zhang, K Pattipati. A rough set theory-based fault diagnosis method for an electric power steering system. *IEEE/ASME Transactions on Mechatronics*, 2018, 23(5): 2042-2053.
[21] D Blana, R Kirsch, E K Chadwick. Combined feedforward and feedback control of a redundant, nonlinear, dynamic musculoskeletal system. *Medical & Biological Engineering & Computing*, 2009, 47(5): 533-542.
[22] X Zhe, X W Min, W Yang, et al. Design of direct yaw moment control system to enhance vehicle stability based on fuzzy logic. *Advanced Materials Research*, 2012, 383-390: 1326-1332.
[23] R Fruqon, Y J Chen, M Tanaka. An SOS-based control Lyapunov function design for polynomial fuzzy control of nonlinear systems. *IEEE Transactions on Fuzzy Systems*, 2017, 25(4): 775-787.
[24] C H Lu, J Zhang. Design and simulation of a fuzzy-PID composite parameters' controller with MATLAB. *2010 International Conference on Computer Design and Applications*, Qinhuangdao, China, 25-27 June, 2010.
[25] H J Lin, Z S Teng, T Chen, et al. Improved fuzzy control method for temperature in water tank of intelligent viscometer. *2008 International Conference on Information and Automation*, Changsha, China, 20-23 June, 2008.
[26] L Lu, B Yao, Q F Wang, et al. Adaptive robust control of linear motor systems with dynamic friction compensation using modified LuGre model. *2008 IEEE/ASME International Conference on Advanced Intelligent Mechatronics*, Xian, China, 2-5 July 2008.
[27] D Y Hou. Integrated direct/indirect adaptive robust control of turntable servo system based on LuGre model friction compensation. *2016 31st Youth Academic Annual Conference of Chinese Association of Automation (YAC)*, Wuhan, China, 11-13 Nov. 2016.